Catalysis Today 175 (2011) 72–77

Contents lists available at ScienceDirect

Catalysis Today

journal homepage: www.elsevier.com/locate/cattod

Support effect on the NO_x storage and sulfur-resisting performance of the NO_x trap catalysts $Pt/Li/TiO_2–MO_x$ (M = Al, Zr, Si, Sn)

Ming Meng*, Lihong Guo, Junjun He, Youlei Lai, Zhaoqiang Li, Xingang Li

Tianjin Key Laboratory of Catalysis Science and Engineering, School of Chemical Engineering and Technology, Tianjin University, Tianjin 300072, PR China

ARTICLE INFO

Article history:
Received 30 October 2010
Received in revised form 30 January 2011
Accepted 26 February 2011
Available online 3 April 2011

Keywords:
Lithium
$TiO_2–MO_x$(M = Al Zr Si Sn) oxides
NO_x storage
Sulfur-resistance
Pt dispersion

ABSTRACT

A series of Li-based lean-burn NO_x trap (LNT) catalysts $Pt/Li/TiO_2–MO_x$ (M = Al, Zr, Si, Sn) were prepared by sequential impregnation with the supports $TiO_2–MO_x$ synthesized by co-precipitation. The support effect on the NO_x storage and sulfur-resisting performance of $Pt/Li/TiO_2–MO_x$ catalysts was investigated carefully. The NO_x storage capacity of fresh $Pt/Li/TiO_2$ is greatly improved by doping with Al_2O_3 or ZrO_2 due to the remarkably increased specific surface area and the oxidation ability of the catalysts. HR-TEM and H_2-chemisorption results reveal that the oxidation ability of $Pt/Li/TiO_2–MO_x$ is mainly determined by Pt crystallite size. Larger Pt crystallites correspond to stronger oxidation ability. The regeneration of sulfated $Pt/Li/TiO_2–MO_x$ strongly depends on the total acidity of the supports, including Brønsted and Lewis acid; the supports with larger acidity possess higher ability of sulfur-resistance and regeneration. The results of in situ DRIFTS show that over $Pt/Li/TiO_2–MO_x$ (M = Al, Zr, Si, Sn) NO_x is mainly stored as ionic nitrate species at 350 °C. Taking the NSC and regeneration ability into account, the catalyst $Pt/Li/TiO_2–Al_2O_3$ is the most promising one for practical application.

1. Introduction

Lean-burn combustion is a promising technology to increase fuel efficiency and decrease the emission of hydrocarbons and carbon monoxide. However, under lean-burn condition more nitrogen oxides (NO_x) are formed, which cannot be effectively removed by conventional three-way catalysts (TWCs). Many techniques have been explored to reduce lean-burn NO_x [1–3]. Among them, lean-burn NO_x trap (LNT) technique is considered as the most promising one for the purification of lean-burn NO_x [4].

A typical LNT catalyst often consists of precious metals (e.g., Pt or Rh) as the active components for the capture and oxidation of gaseous NO, alkali or alkaline earth metal oxides as NO_x storage materials (e.g., potassium or barium compounds), and the support with large specific surface area such as alumina. Since sulfur dioxide (SO_2) in the exhaust can readily react with the basic storage materials to form sulfates, LNT catalysts often deactivate very quickly. In addition, the agglomeration of the support and precious metals can also result in the thermal deterioration of LNT catalysts [5]. Therefore, new kinds of LNT catalysts which possess both high sulfur-resisting performance and high thermal stability are required.

The choice of storage medium in LNT catalysts is important. Breen et al. [6] have ever performed thermodynamic calculation to evaluate the effects of gas composition and reaction temperature on the stability of the sulfates and carbonates of alkali metals and alkaline earth metals under oxidizing and reducing conditions. They found that lithium as NO_x storage medium possesses sufficient NO_x storage capacity and higher sulfur tolerance than the others. Moreover, Yamamoto et al. also [7] found that Li_2O additive is favorable to improving the NO sorption capacity of Pt/TiO_2 under both SO_2-free and SO_2-containing atmosphere. Based on these analyses, lithium is selected as the NO_x storage component in this work. Another important component in LNT catalysts is the support. Recent studies have shown that TiO_2 can remarkably improve the sulfur tolerance of LNT catalysts, due to its high acidity/low basicity [8–10]. However, TiO_2 often shows poor thermal stability and low specific surface area [11]. The addition of other metal oxides to TiO_2, such as Al_2O_3 [12], ZrO_2 [5], SiO_2 [13], SnO_2 [14], can effectively modify the surface properties of TiO_2 including specific surface area, pore structure and surface acidity. Up to now, no research has yet been performed to investigate the support effect of TiO_2-based binary oxides on the NO_x storage-reduction behavior of Li-based LNT catalysts. In present work, a series of Li-based LNT catalysts $Pt/Li/TiO_2–MO_x$ using binary oxides $TiO_2–MO_x$ (M = Al, Zr, Si, Sn) as supports were prepared by sequential impregnation. The support effect on the performance of fresh and regenerated catalysts is investigated carefully. The support properties, Pt dispersion

* Corresponding author. Tel.: +86 022 2789 2275; fax: +86 022 2789 2275.
E-mail address: mengm@tju.edu.cn (M. Meng).

0920-5861/$ – see front matter © 2011 Elsevier B.V. All rights reserved.
doi:10.1016/j.cattod.2011.02.051

and catalytic performance of the catalysts are well correlated. The NO_x storage and sulfur poisoning mechanisms over these catalysts are also revealed.

2. Experimental

2.1. Catalyst preparation

Support preparation: mixed oxides gel of TiO_2–MO_x (atomic ratio: Ti/M = 1/1, M = Al, Zr, Si, Sn) was prepared by co-precipitation. Appropriate amounts of $TiCl_4$, $AlCl_3{\cdot}6H_2O$, $ZrOCl_2$, $SnCl_4{\cdot}5H_2O$, $(C_2H_5O)_4Si$ (Guangfu Chemical Reagents Factory of Tianjin) were dissolved in distilled water, then ammonia was added dropwise until the pH arrived at ca. 10. After continuous stirring for 2 h, the formed materials were aged at the synthesis temperature for 24 h without stirring. The obtained precipitate was thoroughly washed with deionized water until no chloride ions in the filtrate could be detected by the $AgNO_3$ solution. Then the obtained cake was dried at 120 °C overnight and calcined in air at 500 °C for 4 h. For comparison, pure TiO_2 was also prepared by the same method.

Catalyst preparation: the catalysts were prepared by sequential impregnation. At first, Pt was loaded onto the supports by impregnating the supports into $H_2PtCl_6{\cdot}6H_2O$ solution. Then the wet precursor was dried at 120 °C overnight and calcined in air at 250 °C for 1 h, in the next, the dried Pt/TiO_2–MO_x was impregnated into an aqueous solution of $LiNO_3$. After dried at the same condition and calcined in air at 500 °C for 2 h, the final catalyst was obtained, which is denoted as Pt/Li/TiO_2–MO_x (M = Al, Zr, Si, Sn). The atomic weight loadings of Pt and Li in the final catalysts are 1% and 4%, respectively. Before experiments, the catalysts with an average size of 40–60 mesh were reduced at 500 °C for 1 h in a gas flow of N_2 + H_2 mixture which contains 10 vol.% H_2. For comparison, the sample Pt/Li/TiO_2 was also prepared by the same method.

2.2. Catalyst characterization

The measurement of the specific surface area (S_{BET}) was carried out at −196 °C on Quantachrome QuadraSorb SI instrument by using the nitrogen adsorption method. The samples were pretreated in vacuum at 300 °C for 8 h before experiments. The S_{BET} was determined from the linear part of the BET curve. The pore diameter distribution was calculated from the desorption branch using the BJH formula.

X-ray diffraction measurement was carried out on an X'pert Pro rotatory diffractometer (PANAlytical) operating at 40 mA and 40 kV using Co $K\alpha$ as radiation source (λ = 0.17890 nm). The data of 2θ from 10 to 90° were collected with the step size of 0.017°.

The acidity of different supports was measured by NH_3 temperature-programmed desorption (NH_3-TPD). It was conducted in a home-made conventional flow apparatus equipped with a thermal conductivity detector (TCD). Each time, 300 mg of the support were pretreated at 500 °C under a helium flow (50 mL/min) for 0.5 h and then exposed to a gas mixture of 5 vol.% NH_3/N_2 at 100 °C until the outlet concentration reached the same level as the inlet gas. Thereafter, the inlet gas was switched to flowing helium at 100 °C until no NH_3 was detected in the outlet gas, and then the sample was heated to 600 °C at a rate of 10 °C/min with the TCD signal simultaneously recorded to get the TPD profile.

Pyridine-IR was used to differentiate the kinds of acidic sites on the surface of the supports. Each time, 20 mg of the sample were grounded into fine powder and pressed into very thin self-supporting wafers with a diameter of 13 mm. The disc was mounted in a quartz IR cell equipped with a CaF_2 window and a vacuum system. Prior to adsorption, the samples were pretreated in situ at 350 °C for 1 h under evacuation with the residual pressure of 1.0×10^{-3} Pa; after cooled to 250 °C, the background spectrum was collected by a Nicolet Nexus spectrometer. Pyridine adsorption was performed at 150 °C until the intensity of the spectra was no longer changing. The physically adsorbed pyridine was removed by evacuation for 0.5 h. After the sample was heated to 250 °C in vacuum, the pyridine-IR spectra were recorded.

Temperature-programmed reduction (TPR) was conducted on a TPDRO 1100 apparatus supplied by Thermo-Finnigan Company. Before detection by the TCD, the gas was purified by a trap containing CaO + NaOH materials in order to remove the H_2O and CO_2. Each time, 25 mg of the sample was heated from room temperature to 900 °C at a rate of 10 °C/min. A gaseous mixture of H_2 and N_2 containing 5 vol.% H_2 was used as reductant at a flow rate of 20 mL/min.

H_2-pulse chemisorption was conducted on the same TPDRO1100 apparatus. 200 mg of the sample were heated in pure H_2 from room temperature to 350 °C and held for 30 min. After a subsequent purge in pure helium for 1.5 h, the sample was cooled to room temperature. The H_2 adsorption was performed at room temperature by injection of same dose of H_2 per time until no change in TCD signal was found.

The surface morphology was determined with a Philips XL-30 M scanning electron microscope (SEM) instrument operating at 20 kV. TEM and HR-TEM images were obtained using a Philips Tecnai G^2F20 system operating at 200 kV.

In situ diffuse reflectance infrared spectroscopy (in situ DRIFTS) was measured on a Nicolet Nexus spectrometer equipped with a MCT detector cooled by liquid nitrogen, and an in situ chamber allowing the sample heated up to 600 °C. The NO_x sorption experiments over different samples were carried out at 350 °C. The powder sample (15 mg) was firstly pretreated in helium at 350 °C for 30 min to record the background spectrum, then 400 ppm NO + 5 vol.% O_2 in N_2 with a flow rate of 50 mL/min was introduced into the sample cell. At different exposure times (up to 30 min), the spectra were recorded. By replacing the adsorption gas with 200 ppm SO_2 + O_2, the SO_2 sorption was also carried out. Due to the low concentration of SO_2, the holding time at each temperature is prolonged to 60 min to get stronger signal.

2.3. Sulfur-aging treatment and NO_x storage capacity (NSC) measurement

The sulfur-aging of the fresh catalysts was carried out in a quartz-tubular continuous flow reactor (i.d. = 8 mm). Each time, 400 mg catalyst was exposed to a gas flow (150 mL/min) containing 400 ppm SO_2, 5 vol.% O_2 and the balance N_2 at 400 °C for 3 h. The regeneration of sulfur-aged catalysts (400 mg) was performed in a gas flow of 10 vol.% H_2/N_2 (100 mL/min) in at 500 °C for 60 min.

NSC measurements for both the fresh and regenerated catalysts were carried out in the quartz-tubular continuous flow reactor loaded with 400 mg of each catalyst. After the temperature reached 350 °C, a mixture gas containing 400 ppm NO, 5 vol.% O_2 and balance N_2 was introduced to the reactor at a rate of 400 mL/min, corresponding to a space velocity of 60,000 mL h^{-1} g^{-1}. The concentrations of NO, NO_2 and total NO_x at the reactor outlet were monitored by an online Chemiluminescence NO–NO_2–NO_x Analyzer (Model 42*i*-HL, Thermo Scientific). NSC was calculated by integrating the concentration curves of NO_x as reported elsewhere [15].

3. Results and discussion

3.1. XRD and BET results

The XRD patterns of the fresh samples are shown in Fig. 1. It can be seen that Li_2TiO_3 phase can be detected in all the samples except

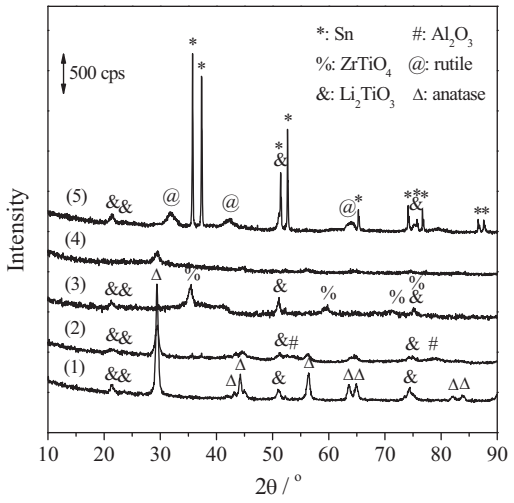

Fig. 1. XRD patterns of the fresh catalysts: (1) Pt/Li/TiO_2; (2) Pt/Li/TiO_2–Al_2O_3; (3) Pt/Li/TiO_2–ZrO_2; (4) Pt/Li/TiO_2–SiO_2; (5) Pt/Li/TiO_2–SnO_2.

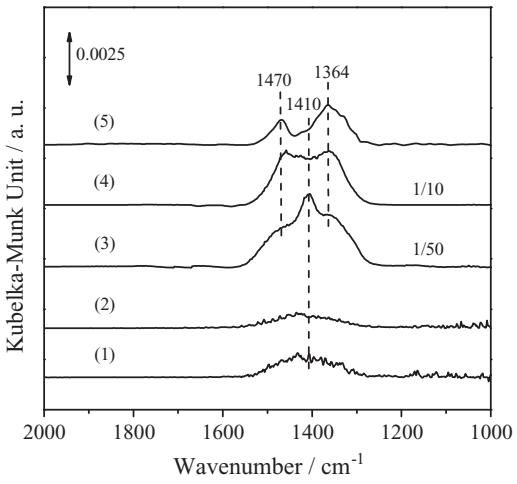

Fig. 2. In situ DRIFT spectra of the catalysts after exposure to 400 ppm NO + 5 vol.% O_2 (balanced by N_2) at 350 °C for 30 min: (1) Pt/Li/TiO_2; (2) Pt/Li/TiO_2–SnO_2 (3) Pt/Li/TiO_2–Al_2O_3; (4) Pt/Li/TiO_2–ZrO_2; (5) Pt/Li/TiO_2–SiO_2.

Pt/Li/TiO_2–SiO_2. The Zr oxide can react with the Ti oxide to form $ZrTiO_4$, as reported in Pt/Li/TiO_2–ZrO_2 [16]. In Pt/Li/TiO_2–SnO_2, rutile TiO_2 appears, indicating that TiO_2–SnO_2 possesses poor thermal stability [17]. Since the catalysts were pretreated at 500 °C for 1 h in a gas flow of 10 vol.% H_2/N_2, the appearance of metallic Sn is natural. No any Pt phases can be observed for all the samples, due to its low content and high dispersion.

The nitrogen adsorption/desorption isotherms and BJH pore diameter distribution of the catalysts are shown in the supporting materials (Fig. S1). All the catalysts exhibit typical IV shape isotherms [18], with the diameter in the mesoporous range. The texture data of the catalysts and the supports are listed in Table 1. It can be seen that pure TiO_2 exhibits the lowest BET surface area of 76 $m^2\ g^{-1}$ among all the supports. After doped with Li and Pt, the BET surface area and the total pore volume decrease obviously but the average pore diameter increases, which are mainly induced by pore blocking and the disappearance of small pores.

3.2. In situ DRIFTS of NO and O_2 co-adsorption

The NO_x storage mechanism over these Li-based LNT catalysts was characterized by in situ DRIFTS technique. Since Al_2O_3 has shown a great effect on the NO_x storage performance of Pt/Li/TiO_2, the catalyst Pt/Li/TiO_2–Al_2O_3 was selected as a representative for in situ DRIFTS study. The spectra are shown in the supporting materials (Fig. S2). It is clear that at the low temperature of 200 °C, only a very weak band of nitrite species is detected (1255 cm^{-1}) [19]. At higher temperature of 250 °C, nitrite species transform to ionic nitrates (1410 cm^{-1}). With the increase of the temperature to 300 °C, other two bands (1364 and 1470 cm^{-1}) appear, also attributed to ionic nitrates [7]. These bands reach the maximum upon heating to 400 °C, then gradually disappear due to the decomposition of nitrates. The optimal temperature region for NO_x trapping as nitrate should be 350–400 °C, which is similar to that for K-based LNT catalysts [20,21].

Fig. 2 displays the in situ DRIFT spectra of different catalysts after 30 min co-adsorption in NO and O_2 at 350 °C. For Pt/Li/TiO_2 and Pt/Li/TiO_2–SnO_2, they show similar spectra with a broad and weak band of ionic nitrates, appearing at 1410 cm^{-1}. For Pt/Li/TiO_2–MO_x (M = Al, Zr, Si), other two bands at 1364 and 1470 cm^{-1} also assigned to ionic nitrates appear. Over Pt/Li/TiO_2–MO_x (M = Al, Zr, Si, Sn) catalysts these nitrate species should be mainly transformed from Li_2TiO_3 phase, which is the main existing species of Li and has been confirmed by XRD results (see Fig. 1).

3.3. In situ DRIFTS of SO_2 and O_2 co-adsorption

Fig. 3 shows the in situ DRIFT spectra of Pt/Li/TiO_2–MO_x (M = Al, Zr, Si, Sn) after exposure to $SO_2 + O_2$ at 350 °C for 60 min. For Pt/Li/TiO_2, an adsorption band around 1160 cm^{-1} is detected, which corresponds to S–O asymmetric stretching mode in bulk sulfate species [7]. After doped with SnO_2, this band shifts to 1146 cm^{-1}. For Pt/Li/TiO_2–SiO_2 only a very weak band at 1285 cm^{-1} assigned to S=O vibration is observed, suggesting the smallest amount of sulfur species deposited on this catalyst. As for Pt/Li/TiO_2–MO_x (M = Al, Zr), there are two bands appearing at 1210 cm^{-1} and 1160 cm^{-1}, which could be assigned to S=O and S–O vibrations in bulk sulfate species [7]. In a summary, more sulfur species can be deposited in the form of bulk sulfates on Pt/Li/TiO_2 and Pt/Li/TiO_2–MO_x (M = Al, Zr); while on Pt/Li/TiO_2–MO_x (M = Si, Sn), much less sulfate species are formed, which mainly exist as surface sulfate species.

Table 1
Specific surface area (S_{BET}), pore volume (PV) and average pore diameter (APD) of the supports and the corresponding catalysts, and the NO_x storage capacity (NSC) of the fresh and regenerated catalysts.

Sample	S_{BET} ($m^2\ g^{-1}$)	PV ($cm^3\ g^{-1}$)	APD (nm)	NSC ($\mu mol\ g^{-1}$)		RE (%)
				Fresh	Regenerated	
Pt/Li/TiO_2	25.9 (76.3)[a]	0.110 (0.160)[a]	12.4 (6.6)[a]	50	44	88
Pt/Li/TiO_2–Al_2O_3	103.6 (250.7)	0.274 (0.336)	9.4 (4.9)	246	235	95
Pt/Li/TiO_2–ZrO_2	58.6 (262.0)	0.253 (0.393)	12.6 (4.3)	145	138	95
Pt/Li/TiO_2–SiO_2	116.9 (254.7)	0.475 (0.660)	12.4 (9.7)	120	112	93
Pt/Li/TiO_2–SnO_2	52.5 (112.8)	0.170 (0.211)	9.7 (6.6)	66	59	89

RE, recovery efficiency, which is the NSC ratio of the regenerated catalysts to the fresh ones.
[a] The data in the parentheses correspond to the supports.

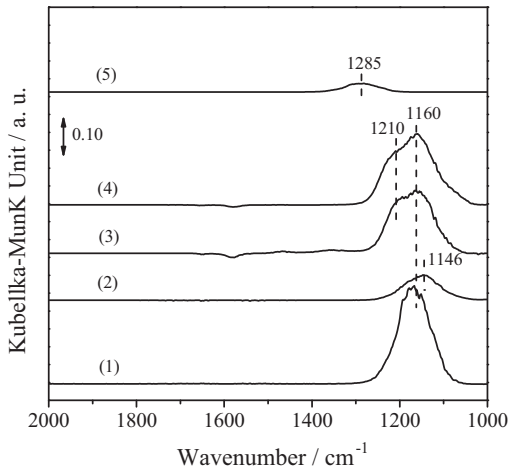

Fig. 3. In situ DRIFT spectra of the catalysts after exposure to 200 ppm SO_2 + 5 vol.% O_2 (balanced by N_2) at 350 °C for 60 min: (1) Pt/Li/TiO_2; (2) Pt/Li/TiO_2–SnO_2 (3) Pt/Li/TiO_2–Al_2O_3; (4) Pt/Li/TiO_2–ZrO_2; (5) Pt/Li/TiO_2–SiO_2.

3.4. Desulfation

To investigate the catalyst regeneration behavior, H_2-TPR experiments were performed on the sulfur-aged catalysts. The results are presented in Fig. 4. For the sulfated catalyst Pt/Li/TiO_2 and those promoted by Al_2O_3 or ZrO_2, the main reduction peak appears at 515 °C. For sulfur-aged Pt/Li/TiO_2–SnO_2, the reduction peak shifts to much higher temperature region (400–700 °C) which includes not only the reduction of sulfates such as Li_2SO_4 but also the reduction of the support SnO_2. As seen in Fig. 1, the metallic Sn can be detected in Pt/Li/TiO_2–SnO_2 after reduction pretreatment [22]. As for Pt/Li/TiO_2–SiO_2, only a small reduction peak at 555 °C is detected, indicating the much less amount of sulfates in this sample, which is consistent with the results of in situ DRIFTS. Compared with the sulfates in conventional Ba-based [23,24] and K-based systems [7], lithium sulfate in Pt/Li/TiO_2 and Pt/Li/TiO_2–MO_x (M = Al, Zr) is much easier to be reduced. For the Li-based LNT catalyst, the regeneration of sulfur aged catalyst is via the formation of H_2S [7], resulting from the reaction between sulfate and hydrogen (reaction (1)) and subsequent hydrolysis reaction between Li_2S and H_2O (reaction (2)). It should be mentioned that the presence of H_2O in real automobile atmosphere will promote the hydrolysis reaction and lower the desorption temperature during the reduction process.

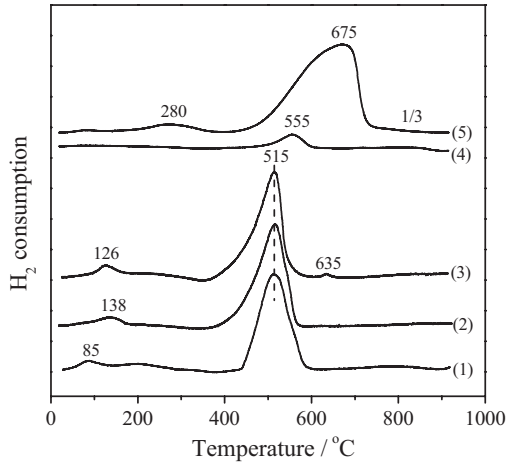

Fig. 4. H_2-TPR profiles of the sulfur-aged catalysts: (1) Pt/Li/TiO_2; (2) Pt/Li/TiO_2–Al_2O_3; (3) Pt/Li/TiO_2–ZrO_2; (4) Pt/Li/TiO_2–SiO_2; (5) Pt/Li/TiO_2–SnO_2.

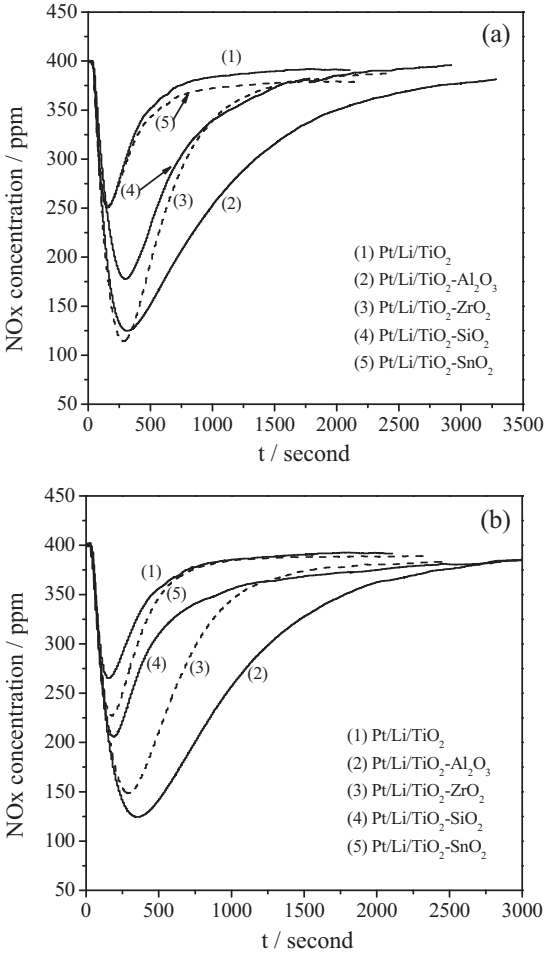

Fig. 5. NO_x storage curves over the fresh (a) and regenerated (b) catalysts at 350 °C (condition: the inlet gas contains 400 ppm NO and 5% O_2, balanced by N_2).

$$Li_2SO_4 + H_2 \rightarrow Li_2S + H_2O \quad (1)$$

$$Li_2S + H_2O \rightarrow Li_2O + H_2S \quad (2)$$

The small reduction peaks below 200 °C for Pt/Li/TiO_2 and Pt/Li/TiO_2–MO_x (M = Al, Zr) can be attributed to the reduction of Pt oxides, which is formed during the oxygen-rich sulfation atmosphere. For SnO_2-promoted sample, this peak shifts to higher temperature (~280 °C), which is resulted from the interaction between the Pt oxide and Sn oxide. The absence of this peak in SiO_2-promoted catalyst suggests that after sulfation the Pt in this catalyst is still in metallic state. For ZrO_2-promoted catalyst there is a very small reduction peak at 635 °C, which can be attributed to the reduction of TiO_2–ZrO_2 support [21].

3.5. NO_x storage behaviors

Isothermal experiments of NO_x storage over all the fresh and regenerated catalysts were carried out at 350 °C, the results of which are shown in Fig. 5(a) and (b), respectively. From Fig. 5(a), it can be seen that at the beginning the NO_x storage is very fast, quickly reaching the lowest point of NO_x concentration; after this the storage rate decreases gradually, with the NO_x concentration increasing slowly until to a steady-state. Similar to the K-based LNT catalysts in previous study [20], the Li species on the catalyst surface are divided into two categories: one adjacent to Pt (I), and another away from Pt (II). The close contact of Pt sites with Li sites (I) can

effectively promote the storage process via oxygen spillover from Pt sites to Li sites, leading to rapid NO_x storage. On the contrary, the transfer of active oxygen species as well as the NO_2 species from Pt sites to Li sites (II) is much slower, leading to the remarkable decrease of NO_x storage rate. Additionally, the NO_x storage performance is also related to the dispersion of Li species. High dispersion of Li species is favorable to rapid NO_x storage. Highly dispersed Li species such as Li_2O and –OLi groups are hard to be detected by XRD, however, their existence cannot be ruled out. On the bulk Li species such as Li_2TiO_3, as confirmed by XRD, the NO_x storage should be much slower due to the surface to bulk diffusion limitation. In a summary, the highly dispersed Li species adjacent to Pt species are more favorable to NO_x storage.

The NO_x storage amounts, calculated by integrating the concentration curves of NO_x, are listed in Table 1. From Table 1, it can be seen that the addition of oxides MO_x (M = Al, Zr, Si, Sn) to $Pt/Li/TiO_2$ can increase its NSC, especially the Al addition, which makes the NSC of $Pt/Li/TiO_2$ increase nearly 4 times. After sulfation and regeneration, the NSC recovery efficiency for this catalyst can reach 95% as seen in Table 1 and Fig. 5(b). For other catalysts $Pt/Li/TiO_2$–MO_x (M = Zr, Si), the NSC recovery efficiency is also higher than 90%. Compared with the Ba-based LNT system [25], the Li-based LNT catalyst possesses better sulfur-resisting and regeneration performance.

It is well known that the NO_x storage performance is highly related to the ability of the catalysts for NO to NO_2 oxidation [26,27]. In this work, during NO_x storage, the concentrations of NO and NO_2 in the feed gas are almost invariable, about 250 and 150 ppm, respectively. Therefore, the change in the concentrations of NO and NO_2 after NO_x storage saturation can reflect the oxidation ability of the catalysts. As shown in Table 2, after storage saturation, the NO_2 concentrations for the fresh catalysts doped with MO_x (M = Al, Zr, Si) are higher than that for the undoped $Pt/Li/TiO_2$, implying their higher oxidation ability, which is consistent with their larger NSC values. After sulfation and regeneration, the oxidation ability of all the catalysts is well maintained. However, their NSC decreases a little. It should be noted that the NSC is related not only to the oxidation ability but also to the available storage sites of the catalysts. The NSC decrease of the regenerated catalysts should be mainly caused by the reduction of basic storage sites.

3.6. Pt dispersion and crystallite size

It has been reported that platinum dispersion (or crystallite size) is a key factor for NO to NO_2 oxidation [27–29]. To make clear that how the oxides MO_x (M = Al, Zr, Si, Sn) affect the oxidation ability of $Pt/Li/TiO_2$, H_2-chemisorption and HR-TEM techniques are employed to characterize the Pt dispersion and Pt crystallite size, respectively. The results are presented in Table 2 and the supporting Fig. S3. H_2-chemisorption results indicate that the addition of promoter oxides to $Pt/Li/TiO_2$ decreases the Pt dispersion, which is consistent with the increase of Pt crystallite size observed from HR-TEM. For the fresh sample $Pt/Li/TiO_2$–SnO_2, the tin exists as metallic state (Fig. 1), which can adsorb and dissociate H_2, so, it is inappropriate to employ H_2-chemisorption to evaluate Pt dispersion in this sample. By calculation of Pt crystallite size and the HR-TEM results, it is found that the Pt crystallites in $Pt/Li/TiO_2$–SnO_2 and $Pt/Li/TiO_2$ have similar size. However, the Pt dispersion can hardly be correlated with the specific surface area of the catalysts. It should be related to the interactions between Pt and the different supports, similar phenomena have also been found by Benard et al. [30].

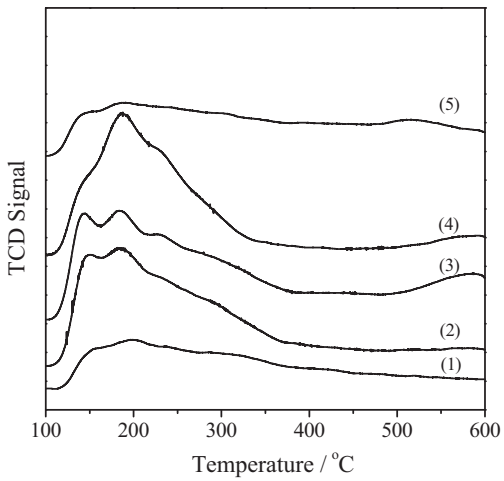

Fig. 6. NH_3-TPD profiles of different supports calcined at 500 °C. (1) TiO_2; (2) TiO_2–Al_2O_3; (3) TiO_2–ZrO_2; (4) TiO_2–SiO_2; (5) TiO_2–SnO_2.

Combining the results of H_2 chemisportion and HR-TEM, it is suggested that the decrease of Pt dispersion and the formation of larger Pt crystallites facilitate the oxidation of NO to NO_2. There are two reasons to explain this. Firstly, based on the calculation results by density function theory (DFT) [31], the oxidation of NO is energy preferred on flat Pt{1 1 1} surface than on stepped Pt{2 1 1} surface. Since Pt{1 1 1} surface dominates in large platinum crystallites, it is proposed that large platinum crystallites are more active for NO oxidation than small crystallites. Secondly, too small Pt crystallites are more easily oxidized to oxides than big ones in the presence of O_2, resulting in further loss of NO oxidation reactivity [28]. In the light of availability of Pt, the reaction is possibly structure-sensitive. Hao et al. also reported that unsupported platinum clusters with ca. 3 nm size are most active for NO oxidation based on a magic cluster model [29]. In this work, the larger platinum crystallites still less than 3 nm show higher oxidation ability is in good agreement with the literature [27–29].

3.7. Acidity of the supports (NH_3-TPD and pyridine-IR results)

It is known that the acidity of the support is beneficial to sulfur-resistance of LNT catalysts [32,33]. Therefore, NH_3-TPD tests were performed on TiO_2 and the promoted supports, as shown in Fig. 6. It is found that the total amount of the desorbed NH_3 increases in the following order:

Table 2
Outlet concentrations of NO, NO_2 and NO_x after NO_x storage saturation, and the dispersion and crystallite size of Pt.

Sample	Fresh/ppm			Regenerated/ppm			Pt dispersion[a]	Dp/nm
	NO	NO_2	NO_x	NO	NO_2	NO_x		
$Pt/Li/TiO_2$	260	131	391	251	140	391	76%	1.5
$Pt/Li/TiO_2$–Al_2O_3	176	205	381	173	215	388	35%	2.5
$Pt/Li/TiO_2$–ZrO_2	187	200	387	182	202	384	40%	2.5
$Pt/Li/TiO_2$–SiO_2	226	170	396	210	178	388	67%	2.0
$Pt/Li/TiO_2$–SnO_2	257	123	380	248	140	388	–	1.5

Dp: crystallite size of Pt determined by HR-TEM.
[a] Assume H/Pt = 1.

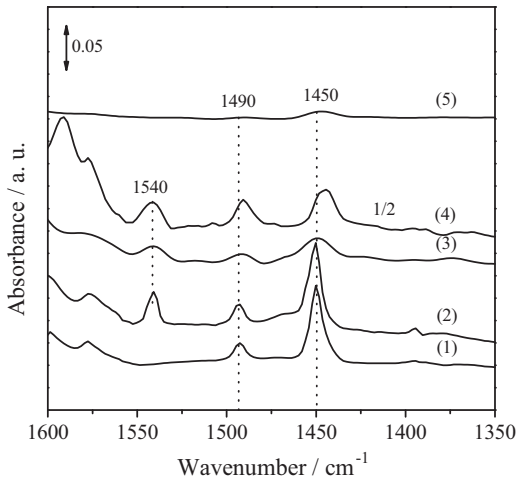

Fig. 7. FT-IR spectra of pyridine adsorption on different supports calcined at 500 °C. (1) TiO_2; (2) TiO_2–Al_2O_3; (3) TiO_2–ZrO_2; (4) TiO_2–SiO_2; (5) TiO_2–SnO_2.

$TiO_2 \approx TiO_2$–$SnO_2 < TiO_2$–$Al_2O_3 \approx TiO_2$–$ZrO_2 < TiO_2$–SiO_2, indicating that the addition of Al, Zr and Si significantly increases the surface acidic sites on the support, which should be caused by the increase of the specific surface area (Table 1) and the interaction between TiO_2 and the promoter oxides MO_x. For example, after the addition of ZrO_2 to TiO_2, a new NH_3 desorption peak above 500 °C can be clearly identified, which is absent for pure TiO_2. So, it is deduced that this peak is related to the interaction between TiO_2 and ZrO_2. Actually, in TiO_2–ZrO_2 supported catalyst a new interaction phase, namely $ZrTiO_4$, has been clearly detected by XRD technique (see Fig. 1).

To distinguish the Brønsted (B) and Lewis (L) acid sites, pyridine IR experiments were performed on the supports. The spectra are presented in Fig. 7. According to literature [34,35], the IR absorption peak at ~1450 cm^{-1} arising from the C–C stretching vibration of a coordinative bonded pyridine complex indicates the presence of L acid sites, while the one at ~1540 cm^{-1} corresponding to the C–C stretching vibration of the pyridine ion suggests the presence of B acid sites. The other one at ~1490 cm^{-1} is contributed by the pyridine species interacting with both B and L acid sites. From Fig. 7, it can be seen that the main acid type on TiO_2 is L acid, giving L and L + B bands at 1450 and 1490 cm^{-1}; while on TiO_2–Al_2O_3, TiO_2–ZrO_2 and TiO_2–SiO_2, B acid sites at 1540 cm^{-1} can also be identified. For TiO_2–SnO_2 support, two very weak bands at 1450 and 1490 cm^{-1} are found, indicating the least surface acid sites in this support. Combined with the acidity of the supports, it is concluded that the NSC and the regeneration performance of the corresponding catalysts Pt/Li/TiO_2–MO_x (M = Al, Zr, Si, Sn) are related to the total acidity of the supports. Larger amount of acidity corresponds to better sulfur resistance.

4. Conclusions

The addition of promoter oxides MO_x (M = Al, Zr, Si, Sn) to TiO_2 can increase the NO_x storage capacity of Pt/Li/TiO_2, especially the Al and Zr addition. The optimal NO_x storage temperature range over Pt/Li/TiO_2–MO_x is 350–400 °C. The main NO_x storage species are ionic nitrates. In situ DRIFTS results reveal that the sulfur poisoning of the catalysts is mainly due to the formation of bulk sulfate species.

The MO_x (M = Al, Zr, Si) addition can remarkably increase the surface area and acidity of the support TiO_2. The NO_x storage capacity of the TiO_2-based LNT catalysts strongly depends on their specific surface area and their ability for NO to NO_2 oxidation, which is mainly determined by the size of Pt crystallites. Too small size of Pt crystallites is unfavorable to NO oxidation. The sulfur resistance and regeneration ability of the TiO_2-based LNT catalysts is related to the total acidity of the corresponding supports. The supports MO_x (M = Al, Zr, Si) with more surface acidic sites show better sulfur-resisting performance. In view of both NO_x storage capacity and sulfur resistance, the Al_2O_3 modified LNT catalyst Pt/Li/TiO_2–Al_2O_3 possesses a great application potential.

Acknowledgements

This work is supported by the National Natural Science Foundation of China (No. 20876110, 21076146), the Specialized Research Fund for the Doctoral Program of Higher Education of China (No. 20090032110013) and the Program of New Century Excellent Talents in University of China (No. NCET-07-0599). The authors are also grateful to the support from "863" Program of the Ministry of Science & Technology of China (No. 2008AA06Z323).

Appendix A. Supplementary data

Supplementary data associated with this article can be found, in the online version, at doi:10.1016/j.cattod.2011.02.051.

References

[1] S. Sato, Y. Yu-u, H. Yahiro, N. Mizuno, M. Iwamoto, Appl. Catal. 70 (1991) L1–L5.
[2] Y. Kintaichi, H. Hamada, M. Tabata, M. Sasaki, T. Ito, Catal. Lett. 6 (1990) 239–244.
[3] R. Burch, P.J. Millington, Catal. Today 26 (1995) 185–206.
[4] T. Kanazawa, Catal. Today 96 (2004) 171–177.
[5] E. Fridell, H. Persson, L. Olsson, B. Westerberg, A. Amberntsson, M. Skoglundh, Top. Catal. 16/17 (2001) 133–137.
[6] J.P. Breen, M. Marell, C. Pistarino, Catal. Lett. 80 (2002) 123–128.
[7] K. Yamamoto, R. Kikuchi, T. Takeguchi, K. Eguchi, J. Catal. 238 (2006) 449–457.
[8] K.M. Adams, G.W. Graham, Appl. Catal. B 80 (2008) 343–352.
[9] M. Casapu, J. Grunwaldt, M. Maciejewski, M. Wittrock, U. Göbel, A. Baiker, Appl. Catal. B 63 (2006) 232–242.
[10] H. Imagawa, T. Tanaka, N. Takahashi, S.I. Matsunaga, A. Suda, H. Shinjoh, Appl. Catal. B 86 (2009) 63–68.
[11] K.I. Hadjiivanov, D.G. Klissurski, Chem. Soc. Rev. 25 (1996) 61–69.
[12] J. Escobar, J.A. De los Reyes, T. Viveros, Ind. Eng. Chem. Res. 39 (2000) 666–672.
[13] N. Economidis, R.F. Coil, P.G. Smirniotis, Catal. Today 40 (1998) 27–37.
[14] Z.M. Liu, K.S. Oh, S.I. Woo, Catal. Lett. 106 (2006) 35–40.
[15] X.X. He, M. Meng, J.J. He, Z.Q. Zou, X.G. Li, Z.Q. Li, Z. Jiang, Catal. Commun. 12 (2010) 165–168.
[16] B.M. Reddya, B. Chowdhury, P.G. Smirniotis, Appl. Catal. A 211 (2001) 19–30.
[17] M.H. Zhou, J.G. Yu, S.W. Liu, P.C. Zhai, L. Jiang, J. Hazard. Mater. 154 (2008) 1141–1148.
[18] K.S.W. Sing, D.H. Everett, R. Haul, L. Moscou, R.A. Pierotti, J. Rouqué rol, Pure Appl. Chem. 57 (1985) 603–619.
[19] Y. Su, M.D. Amiridis, Catal. Today 96 (2004) 31–41.
[20] Y. Liu, M. Meng, Z.Q. Zou, X.G. Li, Y.Q. Zha, Catal. Commun. 10 (2008) 173–177.
[21] Z.Q. Zou, M. Meng, X.Y. Zhou, X.G. Li, Y.Q. Zha, Catal. Lett. 128 (2009) 475–482.
[22] Y.H. Fu, H.C. Ma, Z.L. Wang, W.C. Zhu, T.H. Wu, G.J. Wang, J. Mol. Catal. A: Chem. 221 (2004) 163–168.
[23] S. Matsumoto, Y. Ideka, H. Suzuki, M. Ogai, N. Miyoshi, Appl. Catal. B 25 (2000) 115–124.
[24] C. Sedlmair, K. Seshan, A. Jentys, J.A. Lercher, Catal. Today 75 (2002) 413–419.
[25] J.J. He, M. Meng, Z.Q. Zou, X.X. He, Catal. Lett. 128 (2010) 234–242.
[26] Z.Q. Zou, M. Meng, N. Tsubaki, J.J. He, G. Wang, X.G. Li, X.Y. Zhou, J. Hazard. Mater. 170 (2009) 118–126.
[27] E. Xue, K. Seshan, J.R.H. Ross, Appl. Catal. B 11 (1996) 65–79.
[28] L. Olsson, E. Fridell, J. Catal. 210 (2002) 340–353.
[29] L.D. Li, Q. Shen, J. Cheng, Z.P. Hao, Appl. Catal. B 93 (2010) 259–266.
[30] S. Benard, L. Retailleau, F. Gaillard, P. Vernoux, A. Giroir-Fendler, Appl. Catal. B 55 (2005) 11–21.
[31] Z.P. Liu, S.J. Jenkins, D.A. King, J. Am. Chem. Soc. 125 (2003) 14660–14661.
[32] K. Ito, S. Kakino, K. Ikeue, M. Machida, Appl. Catal. B 74 (2007) 137–143.
[33] N. Takahashi, A. Suda, I. Hachisuka, M. Sugiura, H. Sugiura, H. Shinjoh, Appl. Catal. B 72 (2007) 187–195.
[34] A. Maijanen, E.G. Derouane, J.B. Nagy, Appl. Surf. Sci. 75 (1994) 204–212.
[35] F. Jin, Y.D. Li, Catal. Today 145 (2009) 101–107.